RSC Advances

PAPER

View Article Online
View Journal | View Issue



Cite this: *RSC Adv.*, 2017, **7**, 870

# Effects of mesoporous calcium magnesium silicate on setting time, compressive strength, apatite formation, degradability and cell behavior to magnesium phosphate based bone cements

Liehu Cao,†[a] Weizong Weng,†[a] Xiao Chen,[a] Jun Zhang,[a] Qirong Zhou,[a] Jin Cui,[a] Lin Wang,[a] Jung-Woog Shin[b] and Jiacan Su*[a]

Received 20th October 2016
Accepted 22nd November 2016

DOI: 10.1039/c6ra25503e

www.rsc.org/advances

Mesoporous calcium magnesium silicate was doped into magnesium phosphate to fabricate magnesium phosphate based composite cements (MBC). The results showed that the setting time was significantly prolonged from 4 min to 11 min while the compressive strength decreased from 17 MPa to 9 MPa. In addition, the apatite formation ability improved in simulated body fluid (SBF) and degradation of the composite cements in Tris–HCl solution increased with the increase of m-CMS content of the MBC. Importantly, the MBC with excellent cytocompatibility remarkably promoted the MC3T3-E1 cells proliferation and differentiation, which depended on the m-CMS content. It can be suggested that MBC with good bioactivity, degradability and cytocompatibility has great potential to serve as implanted cements for bone defect filler and repairs.



## Introduction

Magnesium based cement (MPC) is a rapid-setting biomaterial for bone defect filler and repairs, which has the characteristics of fast hardening and high early compressive strength.[1] In the past few years, increasing attention has been paid to MPC for bone defect repairs. Previous studies have showed that the MPC not only had excellent bioactivity to induce apatite formation on its surface but also had good biocompatibility and degradability without mutagenicity and carcinogenicity responses when implanted *in vivo*.[2–6] In addition, the MPC could be degradable both *in vitro* and *in vivo* and released magnesium (Mg) ion to improve the osteoblasts functions. However, the setting time of MPC, ~3 min, is too short, seriously limiting the further application of MPC as a self-hardening cement for bone defects repair in clinic.[7]

Over the past few years, mesoporous materials (pore sizes ranging from 2 to 50 nm) have drawn much attention because of their structural characteristics of tunable pore size, high specific surface area/pore volume, which are expected to be used in bioactive materials for bone regeneration.[8] The high surface area/pore volume of mesoporous materials resulted from mesopores, which was reported to greatly accelerate the apatites deposition on the material surface both *in vitro* and *in vivo*, and thus improving the bone-forming bioactivity.[9,10] Previous study reported that mesoporous magnesium silicate (m-MS) could be degradable in a Tris-solution, and form apatite on its surface in simulated body fluid (SBF), showing good *in vitro* bioactivity, more importantly, the m-MS improved MC3T3-E1 cells proliferation and differentiation.[11] Consequently, mesoporous biomaterials (such as mesoporous silicate and mesoporous bioactive glass, *etc.*) are believed to be excellent candidate biomaterials for bone regeneration and repair bone defects.[12] However, pure inorganic mesoporous materials face challenges in further application in bone regeneration before formulated into scaffolds or bone cements, the main types of materials, to date, for bone regeneration. Hence, the mesoporous wollastonite–polycaprolactone composite scaffold was fabricated and found to enhance bioactivity and promoted MG63 cell functions.[13] Previous study reported that bone cements of mesoporous magnesium–calcium silicate and calcium sulfate composite could promote bone regeneration.[14] In addition, the mesoporous magnesium–calcium silicate strongly enhanced the *in vitro* apatite formation in SBF, and promoted MC3T3-E1 cell functions. In this study, magnesium phosphate based composite cements (MBC) were fabricated by doping mesoporous calcium magnesium silicate into magnesium phosphate. The compressive strength, setting time, *in vitro* bioactivity and degradability, and MC3T3-E1 cells behaviors to the MBC were investigated.

[a]*Department of Orthopaedics Trauma, Changhai Hospital, Second Military Medical University, Shanghai 200433, China. E-mail: drsujiacan@163.com; Fax: +86-21-81873398; Tel: +86-21-81873400*

[b]*Department of Biomedical Engineering, Inje University, Gimhae, 621-749, Republic of Korea*

† Contribute equally.

## Materials and methods

### Fabrication of m-CMS and MPC powders

The 6 g of P123 (EO20PO70EO20, 5800, Sigma-Aldrich) was dissolved in 217 g of deionized water with 6 g of ethanol and 17 mL of concentrated HCl at 38 °C until clear. Then, 7.939 g of $Mg(NO_3)\cdot 6H_2O$ and 7.311 g of $Ca(NO_3)_2\cdot 4H_2O$ were added to the P123 solution, followed by dropwise addition of 12.9 mL tetraethyl orthosilicate, and then stirred at 38 °C for 5 h. The white the precipitate was washed with deionized water, isolated by centrifugation and dried at 120 °C. Then, the powders were calcinated in the muffle furnace (SX2-2.5-12N, Yiheng, Shanghai, China) to remove the template (P123) and obtain m-CMS powders. The morphology and composition of m-MCS were characterized by transmission electron microscopy (TEM, JEM-2010, JEOL Ltd, Japan) and energy dispersive spectrometry (EDS, JEOL-6360LV, Japan).

### Preparation and characterization of MBC

According to the previous literature,[15] MPC powders were designed based on an acid–base reaction, which was fabricated by mixing MgO and $NH_4H_2PO_4$ powder (molar ratio of 1 : 1). The MBC powders were prepared by mixing the MPC powders with 0 w% m-CMS, 15 w% m-CMS and 30 w% m-CMS, which was listed in Table 1. Then, the mixed powders were mixed with deionized water (P/L, 0.2 g $g^{-1}$) to prepare the cements of MPC (0 w% m-CMS), MBC15 (15 w% m-CMS) and MBC30 (30 w% m-CMS). After stirring for 50 s, the obtained cement paste was added into the molds (stainless steel) with the size of $\Phi$ 10 × 2 mm (under a pressure of 2 MPa). The hardened MPC, MBC15 and MBC30 cements were obtained, after storage in an oven (at 37 °C and 100% humidity) for 7 days. The phase composition and microstructure of the obtained cements were characterized by X-ray diffractometer (XRD; Geigerflex, Rigaku Co. Ltd., Japan) and scanning electron microscopy (SEM; S-3400N, Hitachi, Japan), respectively.

### Setting time and compressive strength

Setting times, defined as the time from the moment water was added into the cement powder to the moment, the heavy needle failed to make obvious indentation on the surface of the specimens, of MPC, CMC15 and CMC30 were tested with a Vicat needle (ISO-9597-1989E). The samples of MPC, CMC15, and CMC30 for compressive strength test were obtained by placing the cement pastes into stainless steel moulds ($\Phi$ 6 × 10 mm) at a temperature of 37 °C and 100% humidity (RH) for 7 days. The compressive strength was measured with a universal testing machine (AG-2000A, Shimadzu) at a speed of 1 mm $min^{-1}$ until failure. In this part, three replicates were carried out for each group, and the results were expressed as mean ± standard deviation (M ± SD).

Table 1 Composition, setting time, and compressive strength of different cements

| Name | m-CMS content (wt%) | Setting time (min) | Compressive strength (MPa) |
|---|---|---|---|
| MPC | 0 | 4 ± 0.5 | 17 ± 0.5 |
| MBC15 | 15 | 7 ± 0.5 | 13 ± 0.5 |
| MBC30 | 30 | 11 ± 0.5 | 9 ± 0.5 |

### Cements soaking into SBF

The assessment of *in vitro* bioactivity of the cements of MPC, CMC15, and CMC30 was carried out in SBFs (pH = 7.4). The samples ($\Phi$ 10 × 2 mm) were immersed in SBF (liquid/cements = 20 mL $g^{-1}$, 37 °C) by shaking. The specimens were collected after soaking in SBF for 7 days, then washed gently with distilled water and dried at 50 °C for 12 h. The surface morphology and composition were determined by SEM, and EDS. The change of ion concentration (Ca, Mg, P and Si) in SBF solution after the samples soaking for different times was determined by inductively coupled plasma-atomic emission spectroscopy (ICP-AES, IRIS 1000, Thermo Elemental, USA).

### Degradation of cements *in vitro*

The degradability of the cements (MPC, CMC15 and CMC30) *in vitro* was determined by testing the weight loss ratio, pH value change and surface morphology change of the cements specimens in Tris–HCl solution (pH = 7.4) at different time. The cement specimens with the size of $\Phi$ 10 × 2 mm were soaked in Tris–HCl solution (at 37 °C, and the ratio of solid to liquid of 0.1 g/20 mL), and the soaked solution was replaced 5 days one time. The samples were taken out from the soaked solution, which were washed with water and dried in an oven (at 80 °C and dried for 8 h). The weight loss ratio of these samples was determined according to the following equation:

$$\text{Weight loss } (\%) = (W_t - W_0)/W_0 \times 100$$

where the starting dry weight is $W_0$ and the dry weight at time $t$ is $W_t$.

A pH meter (PHS-2C, JingkeLeici, Shanghai, China) was used to test the pH change of the Tris–HCl solution after the samples immersion for different time. SEM was applied to observe the surface morphology of the specimens after soaking in Tris–HCl for 5 weeks.

### Cell proliferation, morphology, and ALP activity

To evaluate cytocompatibility of the cements, the MC3T3-E1 cells (Cell Bank of Chinese Academy of Sciences) were cultured on the cements (MPC, MBC15 and MBC30) with the size of $\Phi$ 10 × 2 mm in 24-well plates. Before cell seeding, the cements samples were sonicated in ethanol and an autoclave was applied to sterilize at 120 °C (30 min). The MC3T3-E1 cells were seeded on the cements at a density of ~$10^5$ cells per well (100 μL of Dulbecco Modified Eagle Medium (DMEM, Invitrogen, UK) supplemented with 10% fetal bovine serum (FBS; GibcoBRL, Grand Island, NY, USA) and 1% penicillin/streptomycin). Then the cells were incubated at 37 °C in an atmosphere of 100% humidity with 5% $CO_2$, and the medium was change 2 days for one time. At 1, 3, and 5 days, the cell culture medium was removed and phosphate buffered saline (PBS) was used to gently

rinse the cements samples for three times, then transferred to a new plate with 24 wells, then added 100 μL of culture medium containing 0.5 mg $mL^{-1}$ MTT (Amresco, Solon, OH, USA). The culture medium was replaced by 100 μL of dimethyl sulphoxide (DMSO; Sinopharm, Shanghai, China) after 4 h of incubation, and then the supernatant solution was transferred to a 96-well plate after dissolution of the precipitated formazan. An ELISA plate reader (ELx800, BIO-TEK) was applied to measure the optical density (OD) of each well at 570 nm.

SEM and confocal laser scanning microscope (CLSM; Nikon A1R, Japan) was used to observe the cell morphology at 1, 3, and 5 days. Prior to SEM analysis, the 2.5% glutaradehyde solution was used to fix cells in PBS at room temperature for 1 h and then dehydrated in ascending concentrations of ethanol for 5 min at each concentration (30, 50, 70, 90, 95 100, v/v). The 5 μg $mL^{-1}$ FITC-Phalloidin (Cytoskeleton Inc., America) and 10 μg $mL^{-1}$ DAPI (Beyotime Institute of Biotechnology, China) was applied to stain the cells for 40 min and 8 min, respectively, then the samples were observed with CLSM.

The ALP activity was determined to evaluate osteoblast differentiation on the cements (MPC, MBC15 and MBC30) using an ALP assay kit. Briefly, at 7 and 14 days of cell culturing, then culture medium was removed from the samples and the PBS was used to wash cells. Then, placed 200 μL of 1% Nonidet P-40 (NP-40; Beyotime Institute of Biotechnology, China) into each well and incubated for 1 h to get the cell lysate. The 50 μL of supernatant was transferred to a 96-well plate after centrifugation, which was mixed with 50 μL of 2 mg $mL^{-1}$ *p*-nitrophenylphosphate (Sangon, Shanghai, China) substrate solution (consisting of 0.1 mol $L^{-1}$ glycine and 1 mmol $L^{-1}$ $MgCl_2$), which incubated for 30 min at 37 °C. The 100 μL of 0.1 N NaOH was used to quench the reaction, and a microplate reader (SPECTR Amax 384, Molecular Devices, USA) was used to measure the OD value at a wavelength of 405 nm, which was used to quantify the ALP level. The BCA protein assay kit (Pierce Biotechnology Inc., Rockford, IL, USA) was used to determine the ALP activity, which was expressed as the OD per total protein amount.

### Statistical analysis

Student's *t*-test was used to perform statistical analysis. The results are presented as mean ± standard deviation (SD). Differences are thought statistically significant at $p < 0.05$ or 0.01.

## Results

### Characterization of the m-CMS and cements

Fig. 1a shows the TEM images of m-CMS it can be seen that the m-MCS showed ordered mesoporous channels and uniform pore size. Fig. 1b shows the EDS of m-MCS; clearly, the m-MCS consisted of Ca, Mg and Si elements.

Fig. 2a–d present the XRD spectra of m-CMS, MPC, MBC15, and MBC30. No diffraction peak was found in m-CMS, confirming the amorphous structure. For MPC, the peaks assigned to Struvite ($MgNH_4PO_4 \cdot 6H_2O$) and Schertelite ($Mg(NH_4)_2H_2(PO_4)_2 \cdot 4H_2O$) were identified, coexisting with unreacted MgO, in a good agreement with previous studies.[16] In MBC15 and MBC30, the characteristic peaks were almost identical with MPC and no newly formed phase was found, but the intensity of the MBC peaks significantly reduced with the improvement of m-CMS content, suggesting that adding m-CMS had suppressed the crystallization of the hardened MPC cements.

### Setting time and compressive strength of the cements

The setting time and compressive strength of MPC, MBC15, and MBC30 were listed in Table 1. The setting time of MPC was measured to be 4 min, while MBC15, and MBC30 were 7 min and 11 min, respectively, indicating that adding m-CMS prolonged the setting time of the composite cements. The compressive strength of MPC was determined to be 17 MPa, however, it decreased to 13 MPa and 9 MPa for MBC15, and MBC30, respectively, indicating that adding m-CMS decreased the compressive strength of the composite cements.

### Apatite-formation on cements in SBF

Fig. 3 shows SEM images of surface morphology for the MPC, MBC15, and MBC30 after soaking in SBF for 7 days. The ball-like apatite scattered on MPC surface (Fig. 3a), while a lot of apatite aggregated on the MBC15 surface (Fig. 3b). Obviously, the apatite aggregates almost covered the MBC30 surface (Fig. 3c), which were denser than MBC15 and MPC (dependent on the m-MCS content). The EDS of the MBC30 cements are shown in Fig. 3d, and Ca and P peaks was found. Moreover, the results revealed the mole ratio of calcium to phosphorus was approximately 1.58, confirming the formation of

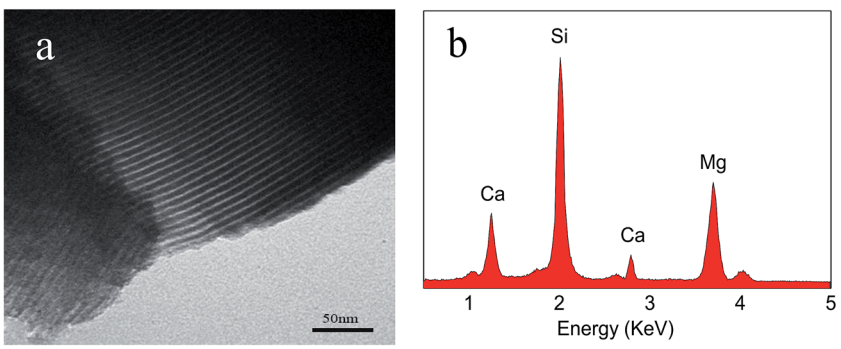


Fig. 1 TEM image (a) and EDS of m-CMS (b).

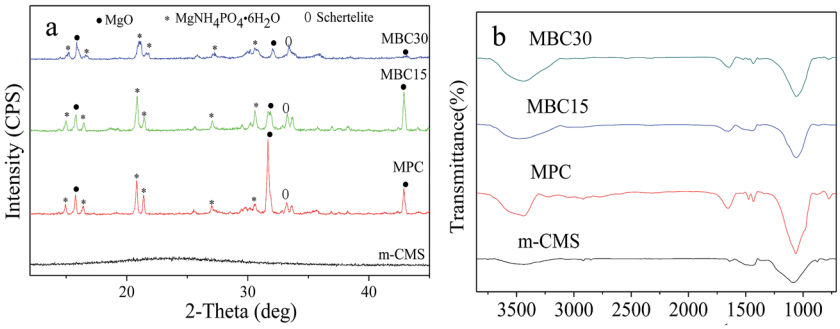


Fig. 2 XRD (a) and IR (b) of m-CMS, MPC, MBC15 and MBC30 after setting for 7 days.

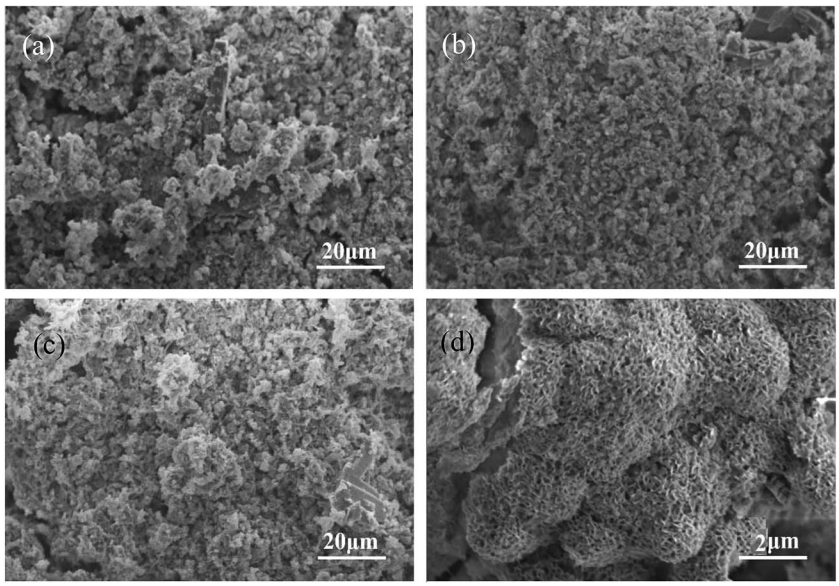


Fig. 3 SEM images of surface morphology of MPC (a), MBC15 (b), MBC30 (c) and MBC30 at higher magnification (d) after immersed in SBF solution for 7 days.

the apatite layer on the MBC30 surface. Fig. 4 reveals changes of Ca, Mg, P and Si ion concentrations in SBF after MBC30 immersion for 14 days. The Ca, P ions gradually in the first 5 days, then slightly increased up to 14 days, while Mg and Si ions sustained increases during the whole mineralization process.

### Degradation of cements *in vitro*

The weight loss ratios of the samples *versus* degradation time were measured as presented in Fig. 5a. Clearly, the samples could degrade in the Tris–HCl solution with time, and the weight loss ratios of MBC30 and MBC15 were 68.2 wt% and 58.3 wt%, respectively, significantly higher than 52.3 wt% for MPC

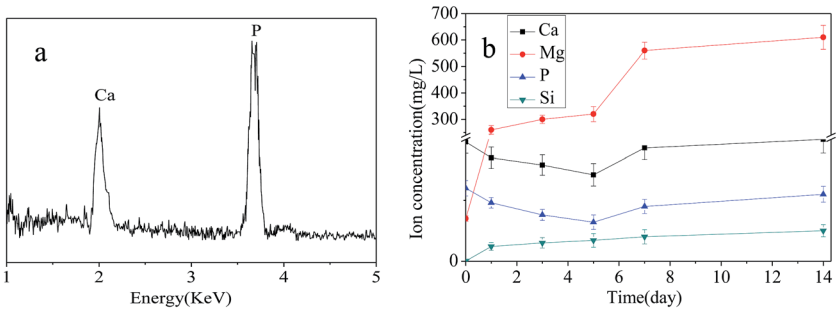


Fig. 4 EDS (a) of the MBC30 after immersed in SBF for 7 days, and changes of ion concentrations in SBF (b) after MBC30 immersion for 14 days.

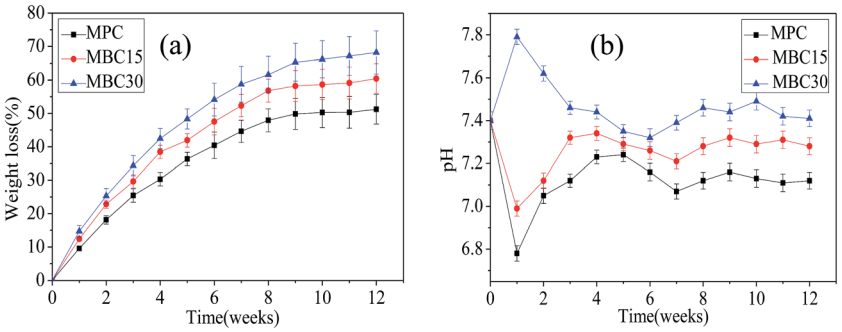


Fig. 5 Weight loss (a) of the samples and pH changes (b) of the solution after MPC, MBC15, and MBC30 soaking into Tris–HCl solution for 12 weeks.

after 12 weeks. Evidently, the incorporation of m-CMS in MPC facilitated the cement degradation and higher percentage of m-CMS in MPC induced faster degradation. Fig. 5b showed the pH changes of the Tris–HCl solution after MPC, MBC15, and MBC30 immersed for different time intervals. The results revealed that the pH value for MBC30 increased from 7.42 to 7.79 during the first week, whereas the values for MBC15 and MPC dropped to 6.98 and 6.81, respectively. Thereafter, it decreased slightly to ~7.41 for MBC30 and increased to ~7.25 and ~7.12 for MBC15 and MPC, respectively in the next 11 week.

Fig. 6 revealed the surface morphology of the MPC, MBC15 and MBC30 before and after immersion in Tris–HCl solution for 5 weeks. The smooth and slippery interfaces on the MPC before immersion in Tris–HCl solution were observed as shown in Fig. 6a, while the MBC15 and MBC30 were covered with some needle-shape bumps in Fig. 6b–c. After 5 weeks, some deep cracks were found on the MPC surface and the surfaces of MBC15 and MBC30 were eroded and formed many micropores as shown in Fig. 6d–f.

### Cell culture on the cements

The optical density (OD) values of the MC3T3-E1 cells cultured on MPC, MBC15 and MBC30 at 1, 3, and 5 days were shown in Fig. 7. No obvious difference could be seen at 1 day among all the samples, while the OD values for MBC15 and particularly

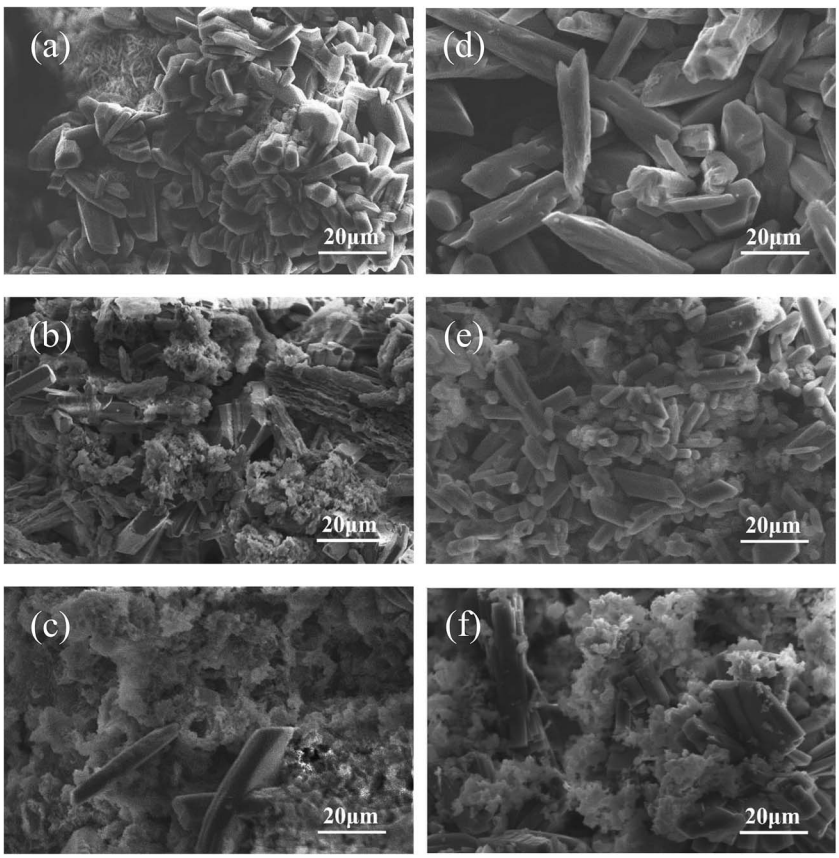


Fig. 6 SEM images of MPC (a and d), MBC15 (b and e) and MBC30 (c and f) before (a–c) and after (d–f) soaking in Tris–HCl solution for 6 weeks.

 

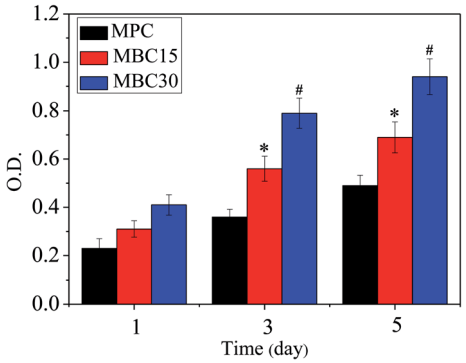


Fig. 7 OD value of MC3T3-E1 cells grew on MPC, MBC15 and MBC30 at 1, 3 and 5 days. *$p$ < 0.05 relative to MBC, #$p$ < 0.01 relative to others.

MBC30 were significantly higher than that for MPC at 3 and 5 days, meaning that cell proliferation was promoted on MBC15 and MBC30.

Fig. 8 and 9 showed the surface morphology, observed by CLSM and SEM, of the MC3T3-E1 cells cultured at 1, 3 and 5 days. Interestingly, the cells exhibited a flattened appearance with more filopodia projecting from the cell body, spreading better on the MBC15 and, particularly, MBC30 surface than on MPC with time. In addition, both CLSM and SEM images showed that cells had increasing density from MPC to composite cements with time, especially MBC30. These findings demonstrated that all samples were biocompatible and the higher percentage of m-CMS incorporated into MPC induced better cell adhesion and spreading.

Fig. 10 showed the ALP activity of MC3T3-E1 cells grew at 7 and 14 days. The ALP activity of the cells increased with time on all samples. Moreover, the ALP activity increased with m-CMS content in composite cements. At 7 days, the ALP activity of the cells grew on the MBC30 was significantly higher than MBC15 and MBC. After cultured for 14 days, the ALP activity of cells on MBC15 was prominently higher than MPC, and it was significantly higher on MBC30 than others.

## Discussions

The MPC can cure with water and form the magnesium ammonium phosphate crystalline in short time, while m-CMS is relatively stable in water. Both the stipe-shaped magnesium ammonium phosphate and the clavate m-CMS were found in the composite cements and clavate-shaped microcrystallines increased with increasing the content of m-CMS. Therefore, it is speculated that the hydraulic reaction of MPC occurred independently and was not influenced by the m-CMS particles, so that the setting time of the composite cements increased with the increase of m-CMS content due to the stable amorphous m-CMS, slowing down the exothermic process and lowering the crystallinity of MPC, as confirmed by the XRD. As a consequence, the setting time improved from 4 min for MPC to 7 min and 11 min for MBC15 and MBC30, respectively. Fast setting is desired, because a long setting time could cause crumbling of

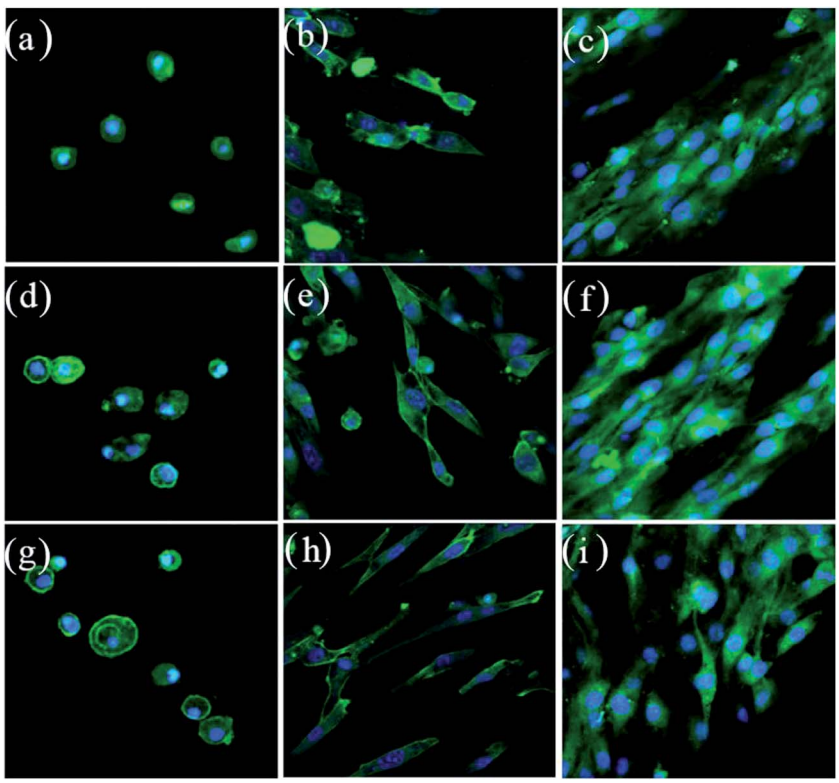


Fig. 8 Confocal images of MC3T3-E1 cells cultured on MPC (a–c), MBC15 (d–f) and MBC30 (g–i) for 1 (a, c, g), 3 (b, e, h), 5 (c, f, i) days.

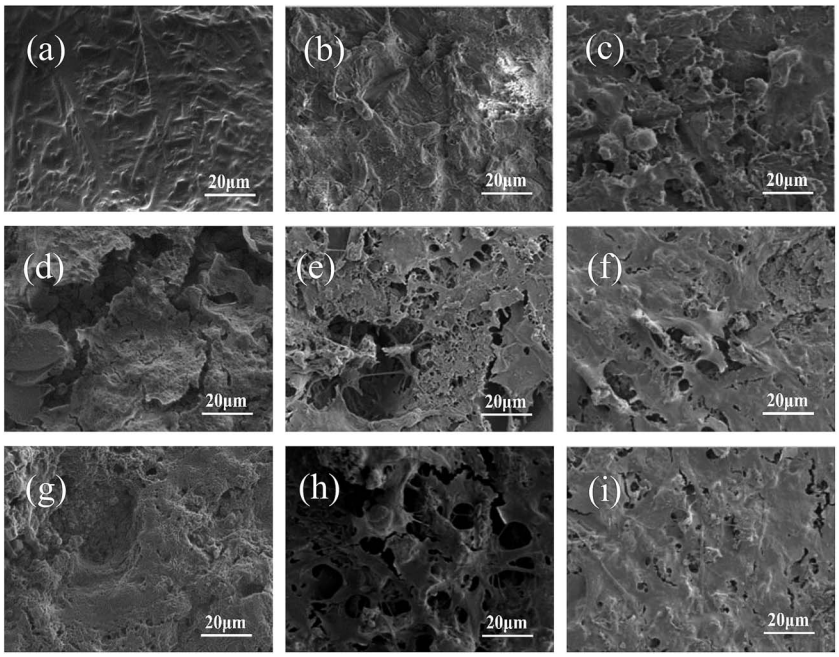


Fig. 9 SEM images of MC3T3-E1 cells cultured on MPC (a–c), MBC15 (d–f) and MBC30 (g–i) for 1 (a, c, g), 3 (b, e, h), 5 (c, f, i) days.

the implanted cement paste in early contact with physiological fluids in some cases, such as the facility of the surgical operation. In general, the appropriate setting time of the bone cement is required to be 8–15 min.[17] Apparently, the setting time of MBC30 fell into the range of 8–15 min, in contrast, the setting times of the MBC and MBC15, even though improved, unmet the general requirement.

To be used for bone defect repair, the bone cements should have not only fast setting process but also adequate compressive strength, which confers immediate load-bearing capacity and mechanical strength resembling the host bone tissue.[18] In addition, early high mechanical strength is necessary to prevent early-stage implant failure or disintegration.[19] The MPC existed in the form of magnesium ammonium phosphate and crystal water, however, the m-CMS destroyed the crystalline of MPC. Therefore, the compressive strength reduced from 17 MPa for MPC to 13 MPa and 9 MPa for MBC15 and MBC30, respectively. Fortunately, the compressive strength of MBC30, although, dropped to 9 MPa, it was, still, good enough for being as bone defects fillers for bone repair.

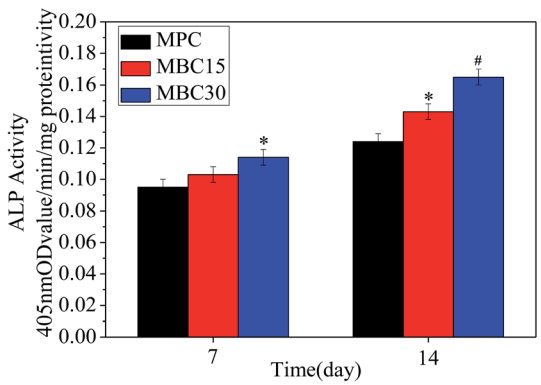


Fig. 10 ALP activity of MC3T3-E1 cells grew on MPC, MBC15, and MBC30 at 7 and 14 days. *$p < 0.05$ relative to MPC, #$p < 0.01$ relative to others.

The hardened MBC15 and MBC30 consisted of magnesium ammonium phosphate ($MgNH_4PO_4$), mesoporous silicate calcium, and magnesium (m-CMS). The appearance of magnesium phosphate was attributed to the acid–base neutralization reactions between MgO and ammonium dihydrogen phosphate.[20] When the molar ratio of 1 : 1 for MgO and $NH_4H_2PO_4$ was used, the final hardened product based the acid–base neutralization reaction was $MgNH_4PO_4$ with 6 crystal water, in accordance with our theoretical design.[21] The characteristic peaks assigned to MBC30 became weaker with the increase of the m-CMS because of the presence of amorphous m-CMS in the cements.

The deposition of apatite on the biomaterials in the biological environment plays an important role in the formation of new bone tissue on the biomaterial surface.[9] A study revealed that the mesoporous materials had a superior ability to induce apatite formation compared with a non-porous structure, resulting from the special mesoporous structure of larger surface area and high pore volume.[10] In this study, the cements could induce apatite deposition within 1 week, which was depending on the m-CMS content, indicating good bioactivity. The excellent bioactivity of cements was attributed to the synergistic effects of Ca with Si ion release from MBC during apatite formation (silicon ions are favourable for the mineralization): as m-MCS gradually degraded, more Ca, Mg and Si ions released and exchanged with $H_3O^+$ in SBF, which facilitates the formation of $HSiO_4^{3-}$, the concentration of silanol groups provided more nucleation sites for apatite. Then, the $Ca^{2+}$, $HPO_4^{2-}$ and $OH^-$ in SBF interacted and finally deposited on the

 

nuclei through a dissolution–deposition process, forming the apatite on MBC surfaces. Therefore, with the significantly improved bioactivity, the CMC30 was expected to have good new bone formation ability.

Bone repair biomaterials should have appropriate degradability, enabling gradually replacement by new bone tissue after implanted *in vivo*.[22] In this study, after immersed in Tris–HCl solution for 12 weeks, the weight loss dramatically increased from 52.3 wt% for MPC to 68.2 wt% for CMC30, revealing that the weight loss of MBC30 was obviously faster than MPC. The m-CMS with unique microstructure features, including high surface area/pore volume, increased the contact area of the m-CMS with liquid after soaked into Tris–HCl solution, thereby leading to faster degradation of MBC30, compared with the MPC. The similar findings were also reported, previously, that modifying the implanted biomaterials with mesoporous structure could improve degradability.[23]

The surface morphology of MBC15 and MBC30 after soaked into Tris–HCl solution for 6 weeks indicated that deep cracks could be seen on the surface. Moreover, due to the surface erosion, some micropores were found on the MBC15 and MBC30, which might further promote the degradation process. The pH of the Tris–HCl solution for the MBC30 rose to 7.79 in the first week, indicating that the m-CMS presented alkaline, and then $NH_4MgPO_4$ degraded into solution generating acidity and inducing the pH increase to 7.41, which might provide a favorable micro-environment for cells growth, proliferation and differentiation.[24]

Generally, bioactive materials for bone regeneration should interact actively with cells and promote cell growth.[25] Mesopours biomaterial was reported to not only improve cell adhesion but also enhance cell proliferation and differentiation.[25,26] In this study, the cell proliferations on MBC15, and especially MBC30 were significantly higher than MPC at 5 days, revealing that MBC15 and MBC30 with a high surface area/pore volume might prominently stimulate cell proliferation as compared with MPC. Besides, the CLSM and SEM images at 5 days also revealed that the MC3T3-E1 cells spread better on MBC15 and MBC30 than MPC, meaning better cytocompatibility of MBC15 and CMC30. The MBC15 and MBC30 with special surface morphology and microstructure, most likely, promote the cells growth duo to the special surface performances of MBC15 and MBC30, which provided a greater chance for the interaction between the cells and cements, thus facilitating cell proliferation. Generally, ALP activity is considered as an indicator of osteogenesis. In this study, the results indicated that the ALP activities of the cells on MBC15, and especially MBC30 were remarkably higher than on MPC at 14 days, indicating that the MBC15 and especially MBC30 promoted the cells differentiation.

The chemical composition of biomaterials plays an important role in governing cellular fate and bio-performances, through controlling the quantity of some useful ions (such as Ca and Mg *etc.*) released from the biomaterials and further influencing the cell–biomaterial interaction.[27] Previous studies indicated that the dissolution products, such as Ca, Si and Mg ions, from bioactive bioglasses and bioceramics stimulated osteoblast proliferation and differentiation.[28] In this study, the Mg, Ca, and Si ions released from the m-CMS, contributing to the enhanced cell proliferation on MBC15, and especially MBC30, as compared with MPC at 7 days. Note that m-CMS with high surface area/pore volume, might release more Mg and Ca ions than MPC and, in pace with gradual degradation, more m-CMS might be exposed to culture medium, which might also occur in degradation study, providing more ions to support cellular events. Hence, it is reasonable that MBC30 with higher m-CMS content revealed better cells responses such as adhesion and proliferation.

Similarly, ALP tests revealed that the MBC15 and especially MBC30 also promoted cell differentiation significantly relative to MPC at 14 days, which can be interpreted in several aspects. First, technically MC3T3-E1 cell differentiation was triggered once confluence achieved during culture, so the better proliferation reached confluence earlier and, automatically, supported better differentiation. The MC3T3-E1 cell proliferation rate was in the order of MBC30 > MBC15 > MPC, therefore, reasonably the MBC30 showed the best differentiation and the MPC showed the lowest differentiation, accordingly. The second factor contributing to the differentiation should be ions, including Ca, P, and Mg. Cellular Ca ion is believed to play an important role in ERK1/2 activation, belonging to extracellular signal-regulated kinases (ERKs), in osteoblasts.[29]

Previous findings suggested that Ca ions influenced mineralization process and ALP activity of MC3T3-E1 cells.[30] As the product in the activity of the tissue non-specific alkaline phosphatase (TNAP), and bone modeling in the bone matrix, P ions also served as a special signal for skeletal cells, regulating cell functions in gene level. Besides, Mg ions are also of importance in bone remodeling and skeletal tissue development of the human body, in particular, involved in the calcification process in calcified tissues. The last but not the least, we should not rule out or ignore the influence of the microstructure generated in MBC30 and MBC15 due to the incorporation of m-CMS into MPC. Numerous studies demonstrated that topography and surface roughness exerted a subtle impact on cellular responses, including adhesion, attachment, proliferation, and mineralization.[31–33] Therefore, it can be concluded that the ions released from m-CMS contributed to the cell proliferation and differentiation.

## Conclusions

Bioactive cements of MBC were fabricated by doping m-CMS into MPC. The cement of MBC30 was easily handled as a cement paste that could set within ~11 min, and the compressive strength achieved 13 MPa. The MBC30 could be degradable in Tris–HCl solution (weight loss ratio of 68.2 wt%) after soaked for 12 weeks. In addition, the MBC30 promoted the MC3T3-E1 cell proliferation as compared with MPC and MBC15, and the cells with normal morphology spread better on MBC30 surface than MBC and MBC15 surfaces. More importantly, the ALP activity of the cells on MBC30 was significantly higher than MPC, indicating that MBC30 could promote cell differentiation. Undoubtedly, the MBC30 with appropriate

setting time and compressive strength showed good bioactivity, degradability and cytocompatibility, which might be an excellent biomaterial pursuing applications for bone repair.

## Acknowledgements

This study was supported by grants from the National Natural Science Foundation of China (31271031, 31100680), the Natural Science Fund of Shanghai (15ZR1412500), the Major International Joint Research Project between China and Korea (81461148033), and the National Research Foundation of Korea (NRF) Grant (NRF-2014K2A2A7066637).



## References

1 E. Champion, Sintering of calcium phosphate bioceramics, *Acta Biomater.*, 2013, **9**, 5855–5875.
2 E. Soudée and J. Péra, Mechanism of setting reaction in magnesia–phosphate cements, *Cem. Concr. Res.*, 2000, **30**, 315–321.
3 D. Zhu and Z. J. Li, High-Early-Strength Magnesium Phosphate Cement with Fly Ash, *Mater. J.*, 2005, **102**, 375–381.
4 M. Wang, Z. Wu and L. Dai, Graphitic carbon nitrides supported by nitrogen-doped graphene as efficient metal-free electrocatalysts for oxygen reduction, *J. Electroanal. Chem.*, 2015, **753**, 16–20.
5 S. Tang, T. Y. Lo, J. M. Horton, C. Bao, P. Tang, F. Qiu, *et al.*, Direct Visualization of Three-Dimensional Morphology in Hierarchically Self-Assembled Mixed Poly(*tert*-butyl acrylate)/Polystyrene Brush-Grafted Silica Nanoparticles, *Macromolecules*, 2013, **46**, 6575–6584.
6 Z. Han, Z. Zhou, X. Shi, J. Wang, X. Wu, D. Sun, *et al.*, EDB Fibronectin Specific Peptide for Prostate Cancer Targeting, *Bioconjugate Chem.*, 2015, **26**, 830–838.
7 Q. Yang and X. Wu, Factors influencing properties of phosphate cement-based binder for rapid repair of concrete, *Cem. Concr. Res.*, 1999, **29**, 389–396.
8 A. S. O. Moscofian, C. R. Silva and C. Airoldi, Stability of layered aluminum and magnesium organosilicates, *Microporous Mesoporous Mater.*, 2008, **107**, 113–120.
9 M. Diba, F. Tapia, A. R. Boccaccini and L. A. Strobel, Magnesium-Containing Bioactive Glasses for Biomedical Applications, *Int. J. Appl. Glass Sci.*, 2012, **3**, 221–253.
10 M. P. Staiger, A. M. Pietak, J. Huadmai and G. Dias, Magnesium and its alloys as orthopedic biomaterials: a review, *Biomaterials*, 2006, **27**, 1728–1734.
11 Z. Wu, T. Tang, H. Guo, S. Tang, Y. Niu, J. Zhang, *et al.*, *In vitro* degradability, bioactivity and cell responses to mesoporous magnesium silicate for the induction of bone regeneration, *Colloids Surf., B*, 2014, **120**, 38–46.
12 X. Gu, Y. Zheng, Y. Cheng, S. Zhong and T. Xi, *In vitro* corrosion and biocompatibility of binary magnesium alloys, *Biomaterials*, 2009, **30**, 484–498.
13 J. Wei, F. Chen, J. W. Shin, H. Hong, C. Dai, J. Su, *et al.*, Preparation and characterization of bioactive mesoporous wollastonite–polycaprolactone composite scaffold, *Biomaterials*, 2009, **30**, 1080–1088.
14 Y. Ding, S. Tang, B. Yu, Y. Yan, H. Li, J. Wei, *et al.*, *In vitro* degradability, bioactivity and primary cell responses to bone cements containing mesoporous magnesium–calcium silicate and calcium sulfate for bone regeneration, *J. R. Soc., Interface*, 2015, **12**(111), 20150779.
15 Z. Chen, X. Li, H. He, Z. Ren, Y. Liu, J. Wang, *et al.*, Mesoporous silica nanoparticles with manipulated microstructures for drug delivery, *Colloids Surf., B*, 2012, **95**, 274–278.
16 M. Y. Riad, S. Shoukry, E. Sosa and G. William, Prediction of concrete initial setting time in field conditions through multivariate regression analysis, *Mater. Struct.*, 2010, **44**, 1063–1077.
17 Y. K. Pan, C. Z. Chen, D. G. Wang and T. G. Zhao, Effects of phosphates on microstructure and bioactivity of micro-arc oxidized calcium phosphate coatings on Mg–Zn–Zr magnesium alloy, *Colloids Surf., B*, 2013, **109**, 1–9.
18 N. Degirmenbasi, D. M. Kalyon and E. Birinci, Biocomposites of nanohydroxyapatite with collagen and poly(vinyl alcohol), *Colloids Surf., B*, 2006, **48**, 42–49.
19 C. M. Murphy, M. G. Haugh and F. J. O'Brien, The effect of mean pore size on cell attachment, proliferation and migration in collagen-glycosaminoglycan scaffolds for bone tissue engineering, *Biomaterials*, 2010, **31**, 461–466.
20 Y. C. Kuo and C. C. Wang, Surface modification with peptide for enhancing chondrocyte adhesion and cartilage regeneration in porous scaffolds, *Colloids Surf., B*, 2011, **84**, 63–70.
21 C. Wu and J. Chang, Degradation, bioactivity, and cytocompatibility of diopside, akermanite, and bredigite ceramics, *J. Biomed. Mater. Res., Part B*, 2007, **83**, 153–160.
22 P. B. Malafaya, T. C. Santos, M. Griensven van and R. L. Reis, Morphology, mechanical characterization and *in vivo* neovascularization of chitosan particle aggregated scaffolds architectures, *Biomaterials*, 2008, **29**, 3914–3926.
23 S. W. Kang, H. S. Yang, S. W. Seo, D. K. Han and B. S. Kim, Apatite-coated poly(lactic-*co*-glycolic acid) microspheres as an injectable scaffold for bone tissue engineering, *J. Biomed. Mater. Res., Part A*, 2008, **85**, 747–756.
24 C. Wu, Y. Zhou, W. Fan, P. Han, J. Chang, J. Yuen, M. Zhang and Y. Xiao, Hypoxia-mimicking mesoporous bioactive glass scaffolds with controllable cobalt ion release for bone tissue engineering, *Biomaterials*, 2012, **33**, 2076–2085.
25 A. I. Moreno-Vega, T. Gomez-Quintero, R. E. Nunez-Anita, L. S. Acosta-Torres and V. Castano, Polymeric and Ceramic Nanoparticles in Biomedical Applications, *J. Nanotechnol.*, 2012, 10.
26 H. Huang, S. Oizumi, N. Kojima, T. Niino and Y. Sakai, Avidin–biotin binding-based cell seeding and perfusion culture of liver-derived cells in a porous scaffold with a three-dimensional interconnected flow-channel network, *Biomaterials*, 2007, **28**, 3815–3823.
27 A. Ito, H. Kawamura, S. Miyakawa, P. Layrolle, N. Kanzaki, G. Treboux, *et al.*, Resorbability and solubility of zinc-containing tricalcium phosphate, *J. Biomed. Mater. Res.*, 2002, **60**, 224–231.

 

28 G. Daculsi, E. Goyenvalle, R. Cognet, E. Aguado and E. O. Suokas, Osteoconductive properties of poly(96L/4D-lactide)/beta-tricalcium phosphate in long term animal model, *Biomaterials*, 2011, **32**, 3166–3177.

29 X. H. Wu, Z. Y. Wu, J. C. Su, Y. G. Yan, B. Q. Yu, J. Wei, *et al.*, Nano-hydroxyapatite promotes self-assembly of honeycomb pores in poly(l-lactide) films through breath-figure method and MC3T3-E1 cell functions, *RSC Adv.*, 2015, **5**, 6607–6616.

30 H. Sowa, H. Kaji, T. Yamaguchi, T. Sugimoto and K. Chihara, SMAD3 promotes alkaline phosphatase activity and mineralization of osteoblastic MC3T3-E1 cells, *J. Bone Miner. Res.*, 2002, **17**, 1190–1199.

31 M. J. Dalby, Topographically induced direct cell mechanotransduction, *Med. Eng. Phys*, 2005, **27**, 730–742.

32 P. M. Davidson, H. Ozcelik, V. Hasirci, G. Reiter and K. Anselme, Microstructured Surfaces Cause Severe but Non-Detrimental Deformation of the Cell Nucleus, *Adv. Mater.*, 2009, **21**, 3586–3590.

33 Z. Zhou, M. Qutaish, Z. Han, R. M. Schur, Y. Liu, *et al.*, MRI detection of breast cancer micrometastases with a fibronectin-targeting contrast agent, *Nat. Commun.*, 2015, **6**, 7984.